COMPARISONS OF DAMAGE TOLERANCE BETWEEN POST-IMPACT FATIGUE AND OPEN-HOLE FATIGUE FOR HIGH TEMPERATURE POLYMER MATRIX COMPOSITES

Kazumi HIRANO
National Institute of Advanced Industrial Science and Technology (AIST)

Keywords: *high temperature polymer matrix composites, fatigue damage tolerance, low-velocity impact damages, post-impact fatigue, open-hole fatigue, stiffness changes*

Abstract

Generally, impact damages have strong influences on not only static strength characteristics but also fatigue damage tolerance behavior. The objective is to investigate the post-impact fatigue behavior and compare the fatigue damage tolerance with those of the open-hole fatigue behavior. Influences of low-velocity impact damages on both residual compressive strength and post-impact fatigue lives were summarized for three kinds of high temperature polymer matrix composite. The correspondence in damage tolerance between post-impact fatigue and open-hole fatigue behavior was discussed on the basis of stiffness changes as a function of fatigue cycle. It was found that the post-impact fatigue lives can be successfully predicted from the normalized S-N curve by considering the reduction of residual compressive strength after impact.

1 Introduction

It is very important for a wide practical use of polymer matrix composites how to ensure the impact damage tolerance for long-term durability and structural integrity. Generally, impact damages have strong influences on not only static strength characteristics but also fatigue damage tolerance behavior. Relatively little information is also available on the post-impact fatigue behavior of high temperature polymer matrix composites in comparison with conventional epoxy matrix composites [1~4].

We have recently done long-term durability researches for high temperature polymer matrix composites in order to finally achieve the development of associated predictive and accelerated test methods and assessment of durability performance for design [5~12]. The objective of this paper is to investigate the post-impact fatigue behavior of three kinds of high temperature polymer matrix composite and compare the damage tolerance with those of the open-hole fatigue behavior. Low-velocity impact damage was introduced into a narrow coupon type laminated specimen and then performed the fully reversed tension-compression fatigue tests. The influences of low-velocity impact damages on residual compressive strength and post-impact fatigue lives are summarized. Then, the correspondence in fatigue failure mechanism between post-impact fatigue and open-hole fatigue behavior was discussed on the basis of the stiffness changes as a function of fatigue cycle. It is found that the stiffness changes correspond to fatigue failure mechanism and residual fatigue lives can be estimated on the basis of the E/E_0 - N/N_f relationship. Finally, it is shown that the post-impact fatigue lives can be successfully predicted from the normalized S-N curve in terms of static strength by considering the reduction of residual compressive strength after impact.

2 Materials and Experimental Procedures

2.1 Materials and Test Specimen

The materials investigated in this research are carbon fiber reinforced toughened bismaleimide matrix composite, G40-800/5260, thermoplastic polyimide matrix composite, IM600/PIXA-M and thermosetting polyimide matrix composite, MR50K/PETI-5. They are laid up into a 32-ply

quasi-isotropic laminate with a $[+45^{\circ}/0^{\circ}/-45^{\circ}/90^{\circ}]_{4s}$ stacking sequence. Mechanical and chemical properties at room temperature [5,6] are summarized in Table 1. These properties also depend on combination of reinforcement carbon fiber and matrix resin. The G40-800/5260 is slightly better than IM600/PIXA-M and MR50K/PETI-5 at room temperature mainly because of good processability and manufacturability.

Post-impact fatigue test specimen is a coupon-type with the same configuration and dimensions (160^{L}x38.1^{W}x$4.4\sim6^{t}$) to open-hole (6.35 mm dia.) fatigue specimen as shown in Fig. 1. They have an original panel thickness ranging from 4.4 to 4.6 mm and unsupported length is 70 mm. After machining from the as-fabricated panels, the impact damage was introduced at the center of specimen. All specimens were nondestructively inspected before testing to document machining defects. There was no biasing of damage developments due to initial defects.

2.2 Low-velocity Impact Test

Impact load was directly applied on a coupon-type specimen by using an instrumented drop-weight impact tester. The test fixture used for the impact portion of this research contained a 30 mm-diameter opening. A free-falling mass impacted at the center of the specimen. The total weight of the impactor with a 12.7 mm diameter steel spherical tup was approximately 19 N. The impact acceleration and impact force were measured using a piezoelectric accelerometer and two strain gages mounted on the impactor. The impact acceleration and impact force were recorded with a conventional digital data acquisition system.

Three series of impact energy per unit thickness of 1668, 3336 and 6672 J/m (equal to 1500 in.lb./in.), which are very low in comparison with an industry standard for evaluating thick, quasi-isotropic laminates, were chosen. Before and after impact, each specimen was non-destructively evaluated to examine the extent of impact damage by laser optical microscope, soft X-ray and C-scanned ultrasonic examinations.

After the low-velocity impact damage, residual compression tests were also conducted without anti-buckling fixture in order to examine impact energy level dependency of residual compressive strength.

2.3 Post-impact Fatigue Test

The post-impact fatigue tests were performed under load controlled-mode with sinusoidal waveform at a constant cyclic frequency of 5 Hz by using the personal computer-controlled MTS Materials Testing System with an environmental chamber. Temperature is kept at 23±1˚C and relative humidity (RH) at 50±2%. All specimens were gripped by hydraulic wedge-type grips and loaded in fully reversed tension-compression fatigue with stress ratio R= -1. The reason is that the tension-compression fatigue has lower lives than tension-tension and compression-compression fatigue. Cyclic stress versus strain curves were also continuously measured by using extensometer (gauge length 25.4 mm) mounted on the specimen side edge, and monitored stiffness changes as a means of evaluating damage accumulation during fatigue cycle.

Open-hole fatigue tests were also conducted under the same fatigue test condition using open-hole fatigue specimen with the same plane configuration and dimensions.

3 Results and Discussion

3.1 Low-velocity Impact Damages and Residual Compressive Strength

3.1.1 Low-velocity impact damages

There is generally much difference in impact damages between impact surface and back surface. It is unsymmetrical that back surface has larger impact damaged area. The plastically deformed area at the impact surface was measured with the use of the laser optical microscope. There is a quite difference in profile, hole-diameter and maximum depth among these materials. The maximum depth and hole-diameter of plastically deformed area versus impact energy relationships are shown in Figs. 2(a) and (b). At lower energy level, there is the almost linear relationship regardless of materials. The G40-800/5260 composite had an even smaller plastically deformed area.

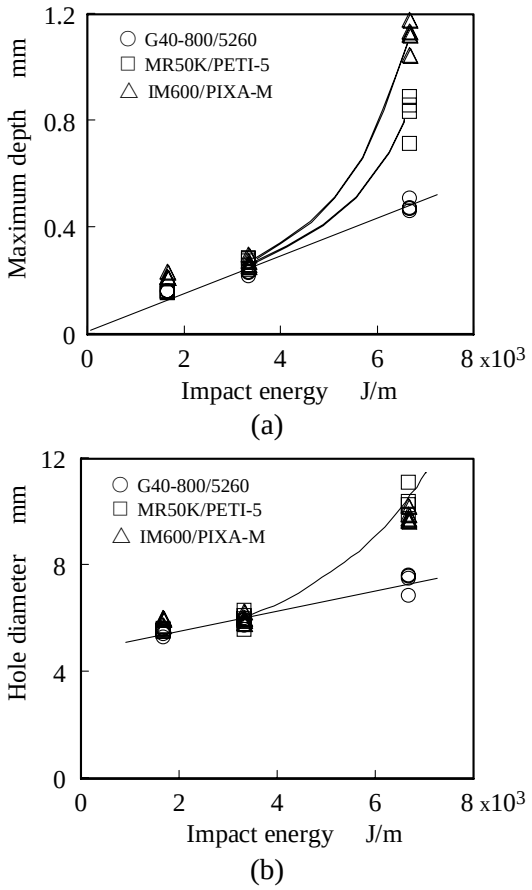

Fig. 2. Maximum depth and hole-diameter versus impact energy relationships

3.1.2 X-ray examinations of internal impact damages

Typical internal damage patterns observed by soft X-ray examination are shown in Figs. 3(a), (b) and (c) for impact energy per unit thickness of 6672 J/m. The toughened G40-800/5260 with a ductile resin had a smaller impact damaged area on the other hand IM600/PIXA-M with a brittle resin had a larger impact damaged area. They had many transverse cracks in every 0˚, ±45˚ and 90˚ laminate layers and de-laminations especially at -45˚/90˚ interlayer. Reinforcement fiber breakages are also partially observed. There is much difference in extents of un-symmetric internal impact damages fundamentally depending on both toughness of matrix resin and inter-lamellar properties. Figure 3 also shows that the impact damage area doesn't spread to whole specimen width within the limits of this experiment.

3.1.3 Residual compressive strength after impact

Residual compressive tests after impact are shown in Figs. 4(a), (b) and (c). These figures show that residual compressive strength decrease with increasing impact energy level and there is no difference in impact energy dependency of residual compressive strength among these materials. The toughened G40-800/5260 with smaller impact damaged area has slightly higher residual compressive strength than IM600/PIXA-M with a larger impact damage area. The MR50K/PETI-5 has a comparable residual compressive strength with G40-800/5260. These tendencies qualitatively correspond to the open-hole compression (OHC) and CAI (compression after impact) characteristics as listed in Table 1.

Macroscopic compressive failure examinations show that failure mode is fundamentally local kink-band formation and internal de-lamination with shear cracks across several plies. However, the out-of-plane bucking induced de-lamination was partially observed at the impact energy level of 1668 J/m. There are some problems in a quantitative determination of residual compressive strength characteristics at lower impact energy level includes the non-impact damaged specimen broken in out-of-plane buckling (see the dotted line drawn in Fig. 4(a)) by the test without anti-buckling fixture.

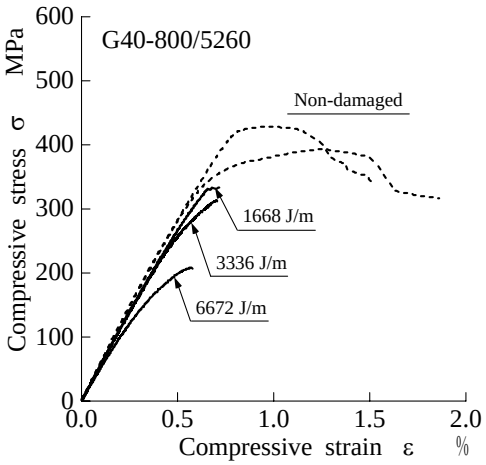

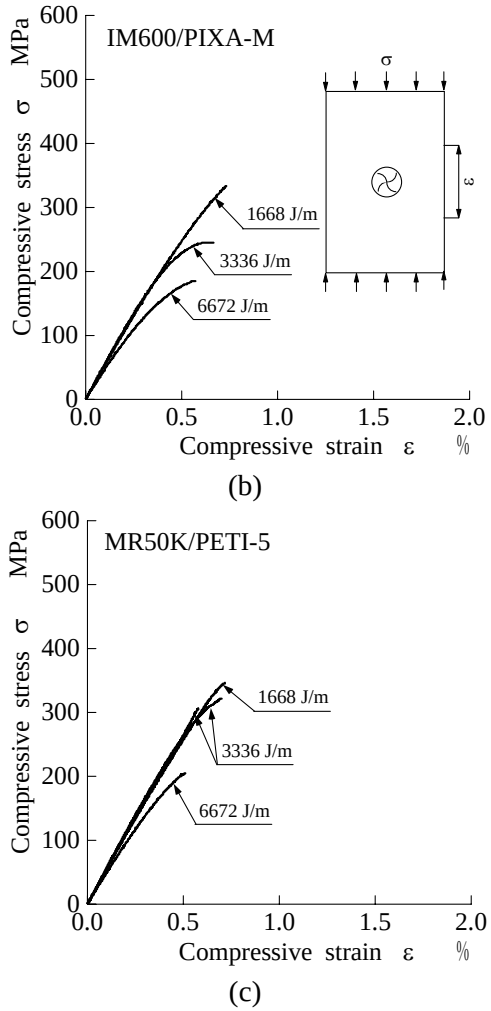

Fig. 4. Residual compressive tests after impact

3.2 Post-Impact Tension-Compression Fatigue

S-N curves of post-impact fatigue are shown in Figs. 5(a) and (b) at low-velocity impact level of 3336 and 6672 J/m, respectively. Minimum (maximum) gross compressive (tensile) stresses σ_{min} (σ_{max}) are plotted against cycles-to-failure N_f (log scale). There is a remarkable influence of low-velocity impact damage on fatigue lives. At 3336 J/m level, the G40-800/5260 has slightly higher fatigue strength than MR50K/PETI-5 but there is little difference in these S-N curves as shown in the straight solid line.

On the other hand, the IM600/PIXA-M with a larger impact damaged area and a lower residual compressive strength after impact has lower fatigue strength than those of the G40-800/5260 and MR50K/PETI-5. And there is a distinguishable knee point in the S-N curve resulted from the transition in fatigue failure mechanism described in details later. Consequently, the post-impact fatigue strength is furthermore very low especially in the high cycle region and the fatigue endurance limit determined at 10^7 cycles is lower than 75 MPa for impact damaged specimen at 6672 J/m. It is summarized here that the G40-800/5260 with smaller impact damaged area and higher residual compressive strength after impact was more resistant to initial impact damage, and more tolerant to fatigue damage after impact.

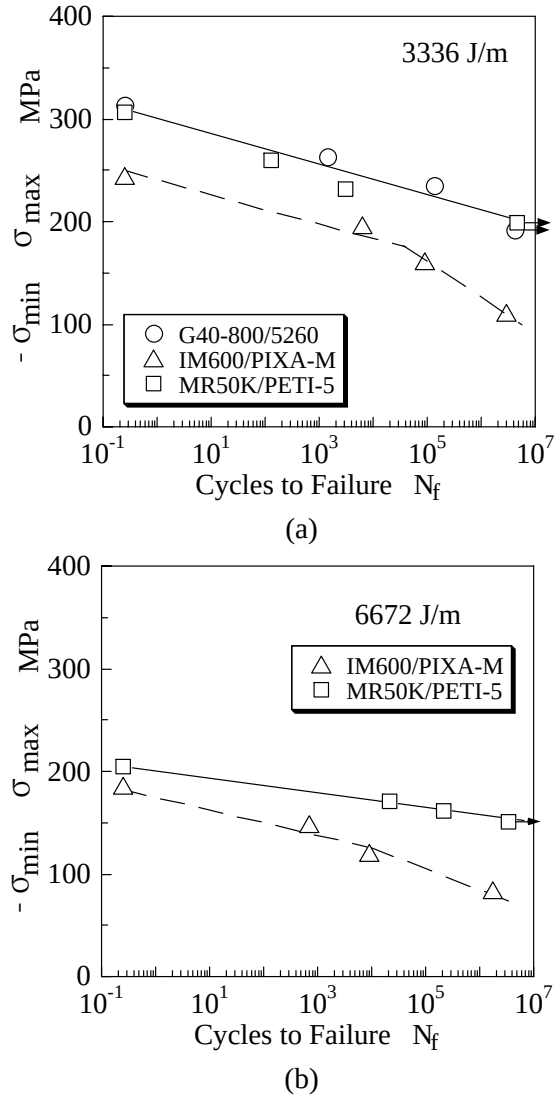

Fig. 5. Materials comparison of S-N curves of post-impact fatigue

Macroscopic examinations of fatigue fracture specimen are shown in Figs. 6(a) and (b) for IM600/PIXA-M and MR50K/PETI-5. These are for impact damaged specimen at 6672 J/m. It is found that post-impact fatigue failure mechanism transits from compressive failure mode with transverse cracking, out-of-plane induced de-lamination and fiber breakages at high applied stress in the low

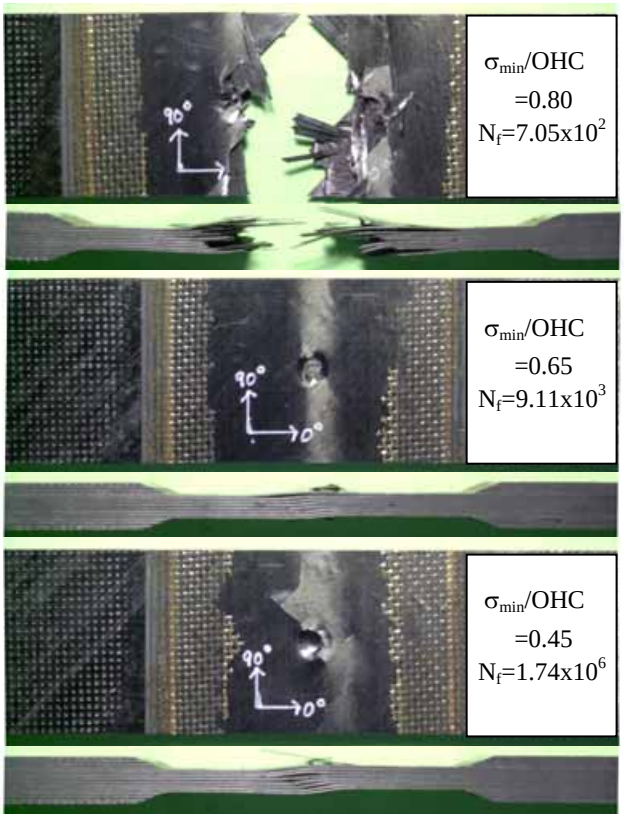

(a) IM600/PIXA-M(6672 J/m)

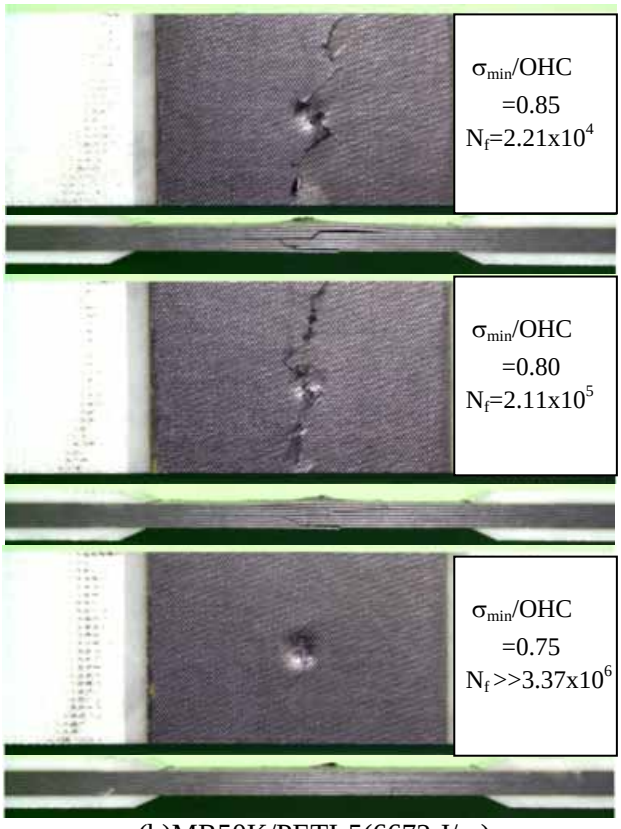

(b)MR50K/PETI-5(6672 J/m)

Fig. 6. Macroscopic examinations of fatigue fracture

cycle region to compressive failure mode with internal de-lamination with shear cracks across several plies at low applied stress in the high cycle region. There is also a quite difference in fatigue failure mechanism between post-impact fatigue and open-hole fatigue. In a case of open-hole fatigue, there is the transition from compressive failure mode at high applied stress in the low cycle region to tensile failure mode with transverse cracking, extensive de-lamination and fiber breakages at low stress in the high cycle region as already reported earlier [13,14].

3.3 Comparisons of Fatigue Damage Tolerance with Open-hole Fatigue

3.3.1 Comparisons of S-N curve

Comparisons of S-N curve between post-impact fatigue and open-hole fatigue are shown in Figs. 7(a), (b) and (c) for G40-800/5260, IM600/PIXA-M and MR50K/PETI-5, respectively. Linear least squares regression fits to the data are also drown. These figures show that there is a remarkable influence of low-velocity impact damage and fatigue lives rapidly decreases with increasing of impact energy. The post-impact fatigue lives at 3336 and 6672 J/m levels are lower than those of open-hole fatigue lives for every material. The IM600/PIXA-M with a larger impact damaged area and a lower residual compressive strength after impact has a great influence and the fatigue endurance limit at 6672 J/m level is lower than 75 MPa.

And it is interesting that G40-800/5260 and IM600/PIXA-M have a distinguishable knee point in the S-N curve at almost the same cycle region ($5x10^4$~10^5 cycles). It is essentially identical to the S-N curve of open-hole fatigue. In a case of open-hole fatigue, it is corresponded to the transition in fatigue failure mode from compressive failure at high applied stress in the low cycle region to tensile failure mode at low applied stress in the high cycle region. As described earlier, the post-impact fatigue failure mechanism transits from compressive failure mode with transverse cracking, out-of plane de-lamination and fiber breakages at high applied stress in the low cycle region to compressive failure mode with internal de-lamination with shear cracks across several plies at low applied stress in the high cycle region. There is also difference in the transition behavior of fatigue failure mechanism between post-impact fatigue and open-hole fatigue. However, it is

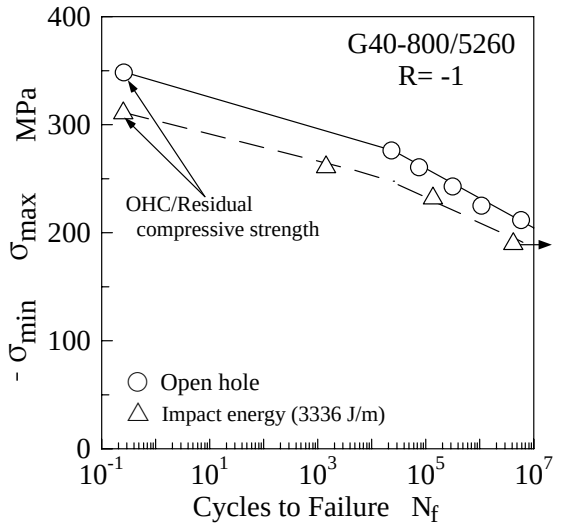

(a)

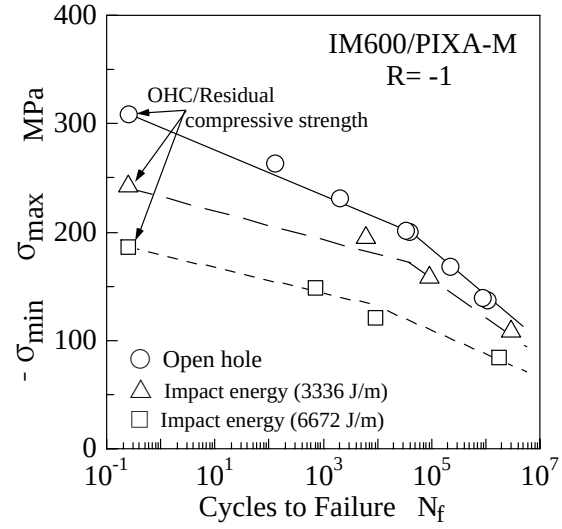

(b)

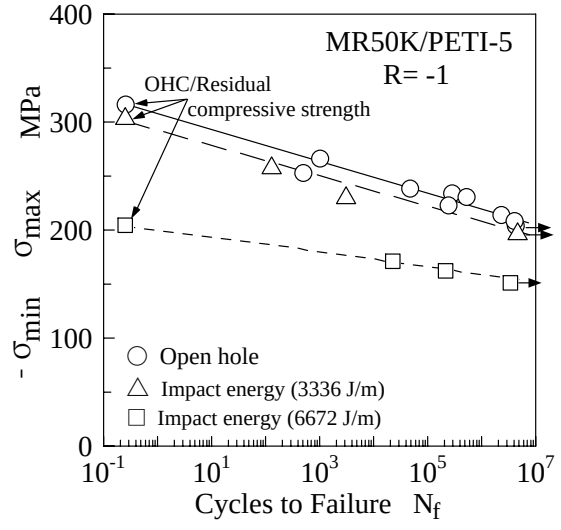

(c)

Fig. 7. Comparisons of S-N curves between post-impact fatigue and open-hole fatigue

presumed that the knee point in the S-N curve for post-impact fatigue is resulted from the transition in the fatigue failure mechanism. On the other hand, the S-N curve for MR50K/PETI-5 is straight line and there is no transition in fatigue failure mode within this experiment as shown in Fig. 6(b).

3.3.2 Stiffness changes as a function of fatigue cycle

An example of comparisons of normalized stiffness changes E/E_0 (E_0 is the average stiffness in the initial 50 cycles) as a function of fatigue cycle N/N_f is shown in Figs. 8 (a), (b) and (c) for IM600/PIXA-M. These are comparisons at roughly 10^3, 10^5 and 10^6 cycle level. The 0-T stiffness denotes the slope in tensile site of cyclic stress versus strain curve and 0-C stiffness the slope in compressive site, respectively. It should be noted here that there is also a difference in applied maximum (minimum) stress between post-impact fatigue and open-hole fatigue, and the stress of post-impact fatigue is lower than that of open-hole fatigue. Generally, it is well known that the stiffness changes fundamentally correspond to micro-cracking, transverse cracking, initiation and propagation of de-lamination and final reinforcement fiber breakage for quasi-isotropic laminate composites.

At low (~10^3) and intermediate (~10^5) cycle region, there is a good correspondence in the 0-C stiffness changes between post-impact fatigue and open-hole fatigue. The compressive fatigue failure is predominately occurred with micro-cracking, transverse cracking, de-lamination and fiber breakages. However, there is a difference in the 0-T stiffness changes. The 0-T stiffness initially decreases slightly and then doesn't change until the final fatigue failure stage with de-lamination and fiber breakages. Therefore the 0-T stiffness doesn't always correspond to damage accumulation behavior during fatigue cycle. The slight decrease at initial 10~20% of N/N_f is also due to micro-cracking and transverse cracking.

At high (~10^6) cycle region, there is a remarkable difference in both the 0-T and 0-C stiffness changes characteristics between post-impact fatigue and open-hole fatigue. It is a reason that compressive failure mode with internal de-lamination with shear cracks across several plies predominantly occurred in post-impact fatigue, on the other hand tensile fatigue failure mode with micro-cracking, transverse cracking and large extent

of de-lamination until the final fiber breakages in open-hole fatigue. It is concluded here that the stiffness changes comparatively correspond to fatigue failure mechanism occurred during fatigue cycle, and residual fatigue lives may also be estimated from the stiffness changes on the basis of the E/E_0 - N/N_f relationships. Similar results are also obtained for G40-800/5260 and MR50K/PETI-5.

3.3.3 Similarity in the normalized S-N curve

The normalized S-N curves in terms of static strength are shown in Figs. 9(a), (b) and (c). The post-impact fatigue is normalized by residual compressive strength after impact and open-hole fatigue by the open-hole compression (OHC), respectively. It is very interesting that there is a respective unique normalized S-N curve between post-impact fatigue and open-hole fatigue regardless of impact energy level. The decreases of fatigue lives fundamentally resulted from the reduction of residual compressive strength after impact damage. Therefore, it is successfully predicted the post-impact fatigue lives from these normalized S-N curve by considering the reduction of residual compressive strength after impact. It is also interesting that there is a distinguishable knee point in the normalized S-N curve for G40-800/5260 and IM600/PIXA-M. It is resulted from the transition in fatigue failure mechanism as described in details. Although there is a little scatter in data, the normalized S-N curve for MR50K/PETI-5 is straight line and there is no transition behavior in fatigue failure mechanism within this experiment.

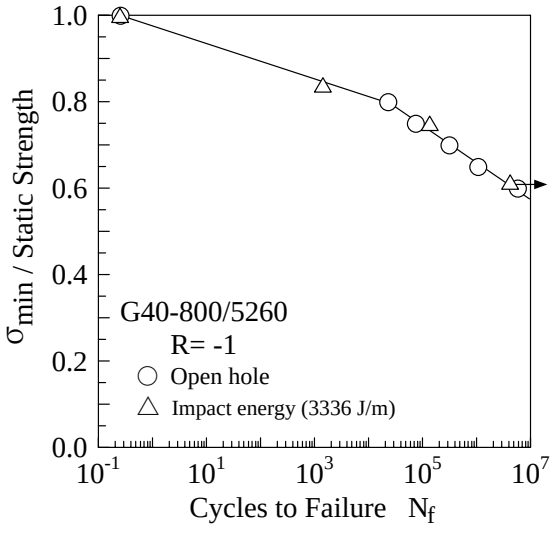

(a)

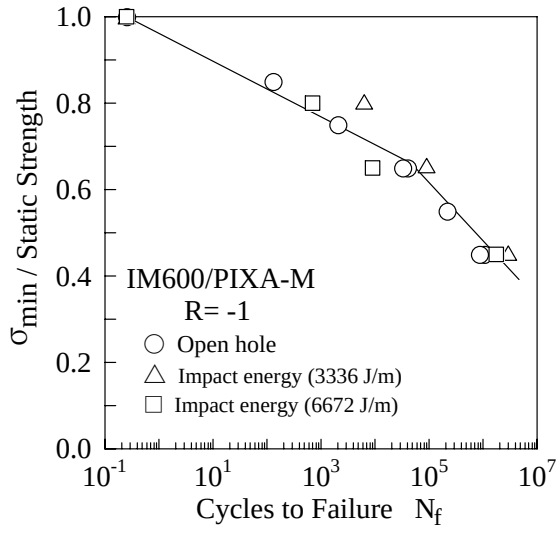

(b)

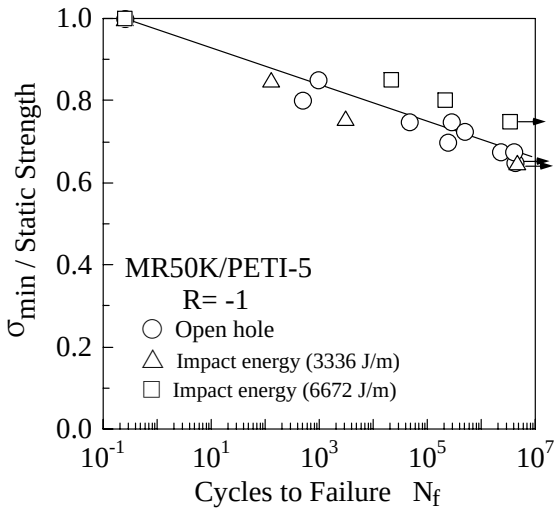

(c)

Fig. 9. Normalized S-N curves

4 Conclusions

The test results obtained here may be summarized as follows;

(1) There is a quite difference in the extent of low-velocity impact damages among the high temperature polymer matrix composites. For low-velocity impact damage, compared on equal impact energy level, the residual compressive strength of the G40-800/5260 is slightly greater than those of the IM600/PIXA-M and MR50K/PETI-5.

(2) There is a remarkable influence of low-velocity impact damage on fatigue lives. The IM600/PIXA-M with a larger impact damaged area and a lower residual compressive strength after impact has lower fatigue lives than those of

the G40-800/5260 and MR50K/PETI-5. The G40-800/5260 composite is more resistant to initial impact damage and more tolerant to fatigue damage after impact.

(3) The stiffness changes correspond to fatigue failure mechanism occurred during post-impact tension-compression fatigue cycle and residual fatigue lives can be estimated on the basis of the E/E_0-N/N_f relationships

(4) Every high temperature polymer matrix composite has a respective unique normalized S-N curve in terms of static strength between post-impact fatigue and open-hole fatigue. It is successfully predicted the post-impact fatigue lives from the normalized S-N curve by considering the reduction of residual compressive strength after impact.

Acknowledgments:

This research had been conducted as a part of Japan Supersonic Research Program under the supports of Ministry of Economy,Trade and Industry. I would like to highly acknowledge all members of Technical Committee of Research Institute of Metals and Composites for Future Industry (RIMCOF).

References

[1] Abrate, S., *Impact on Composite Structures*, Cambridge University Press, Cambridge, UK, pp.206-209, 1998

[2] Ramkumar, R. L., Effect of low-velocity impact damage on the fatigue behavior of graphite/epoxy laminates in *Long Term Behavior of Composites*, ASTM STP 813, O'Brien T. K., ed., pp.116-135, 1983

[3] Portanova, M. A., Poe, C. C., and Whitcomb, J. D., Open hole and post-impact compressive fatigue of stitched an unstitched carbon-epoxy composites in *Composite Materials; Testing and Design*, ASTM STP 1120, Grimes, G. C., ed., pp.37-53, 1992

[4] Lauder, A. J., Amateau, M. F., and Queenay, R. A., Fatigue resistance of impact damaged specimens vs. machined hoe specimens, *Composites*, 24(4), pp.443-445, 1993

[5] Hirano, K., Strategies for R&D on Construction and Preparation of Design Database for Advanced Composite Materials, *J. of the Japan Society for Composite Materials*, Vol.26, No.1, pp.3-8, 2000 (in Japanese)

[6] *NEDO Report*, Studies on Establishment of Long-term Durability Testing and Methodologies for High Temperature Polymer Matrix Composites, March 31, 2000 (in Japanese)

[7] Hirano, K., T. Suzuki, H. Nakayama, M. Noda and Y. Yamaguchi, Thermo-mechanical Response under the Simulated SST Flight Profile and Residual Open-hole Tension-Compression Fatigue Strength for Advanced High Temperature Polymer Matrix Composites, *Durability Analysis of Composite System 2001*, PP.61-69, 2002

[8] Hirano, K., Moisture Absorption Effects on Open-Hole Fully-Reversed Tension-Compression Fatigue Damage Tolerance of High Temperature Polymer Matrix Composites, *Proc. 3rd Japan-Korean Conference on Composite Materials*, 2002

[9] Hirano, K and H. Nakayama, Residual Open-Hole Fatigue Strength after Accelerated Thermal Cycle Aging of High Temperature Polymer Matrix Composites, *Proc. of 10th Japan-US Conference on Composite Materials*, pp.829-838, 2002

[10] Hirano, K., Low-Velocity Impact Damages and Post-Impact Fatigue Behavior for High Temperature Polymer Matrix Composites, *FATIGUE 2002 - Proceedings of the 8th International Fatigue Congress*- Vol. 1, pp.183-190, 2002

[11] K. Hirano, S. Miyake and H. Yoshida, Post-Impact Fatigue Behavior of High Temperature Polymer Matrix Composites, *Proc.10th International Conference on Fracture (ELSEVIER SCIENCE)* in CD-ROM, 2001

[12] K. Hirano, Current Status and Future Prospects of R&D on Construction of Design Database for Advanced Composites and Structures in Japan, *Proc. of 7th Japan International SAMPE Symposium-Information and Innovation in Composites Technologies*, pp.241-244, 2001

[13] Hirano, K., S. Miyake and H. Yoshida, Comparisons of Open-hole Fatigue Strength Characteristics Between Candidate High Temperature Polymer Matrix Composites for the Next Generation Aircraft, *Proc. of Asian Pacific Conference on FRACTURE and STRENGTH'01 (APCFS '01) and International Conference on ADVANCED TECHNOLOGY in EXPERIMENTAL MECHANICS '01 (ATEM'01)*, Vol. 2, pp.593-598, 2001

[14] Hirano, K., Moisture Absorption Effect and Fatigue Damage Tolerance for Advanced High Temperature Polymer Matrix Composites, *Proc. of Composite Durability Workshop CDW2001*, pp.2.1-10, 2001

Table 1. Summary of mechanical and chemical properties at room temperature

	G40-800/5260	IM600/PIXA-M	MR50K/PETI-5
OHT MPa	576	461	426
Tensile modulus GPa	NA	58.2	55.1
OHC MPa	349	309	317
Compressive modulus GPa	57.2	60	53.8
CAI (1500 in.lb/in.)	358	308	298
Tg ℃	206	235	250

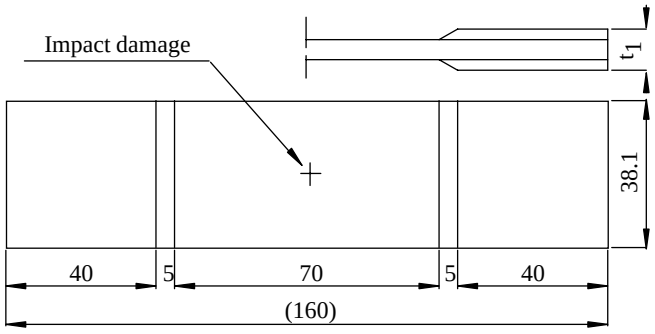

Fig. 1 Configuration and dimensions of post-impact fatigue test specimen

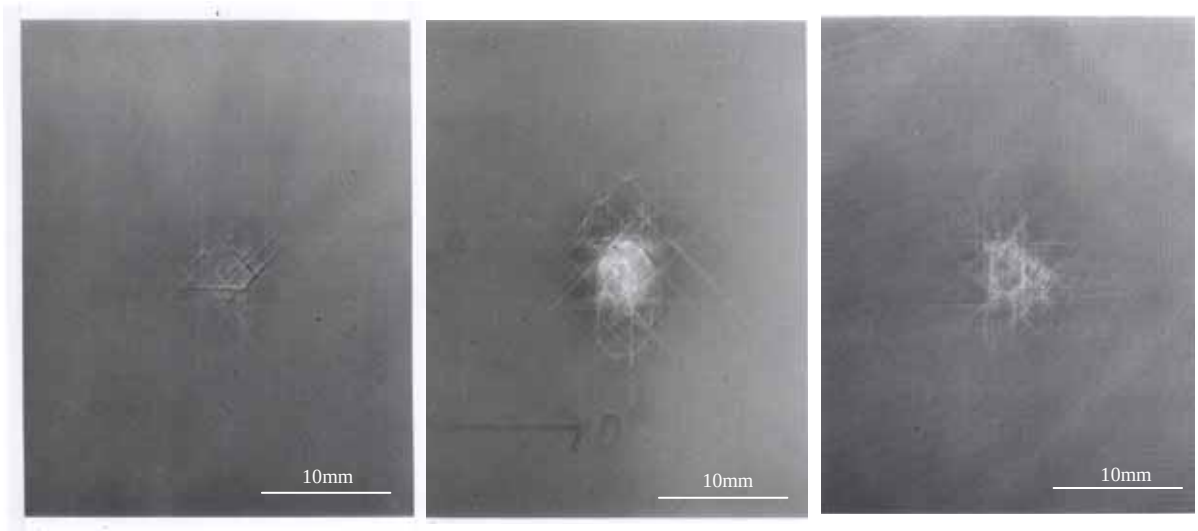

(a)G40-800/5260 (b)IM600/PIXA-M (c)MR50K/PETI-5

Fig. 3 X-ray examinations of internal impact damages (Impact energy per unit thickness: 6672J/m)

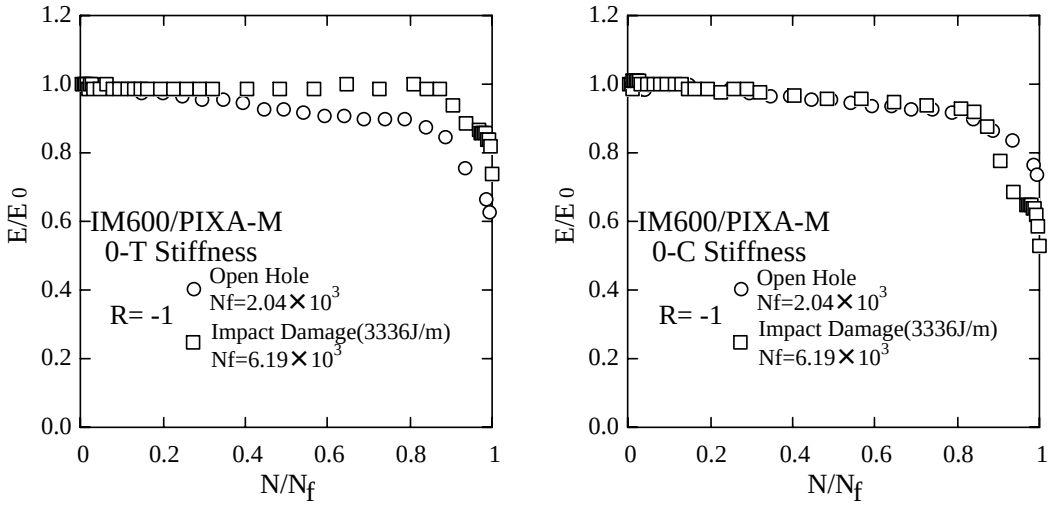

(a)

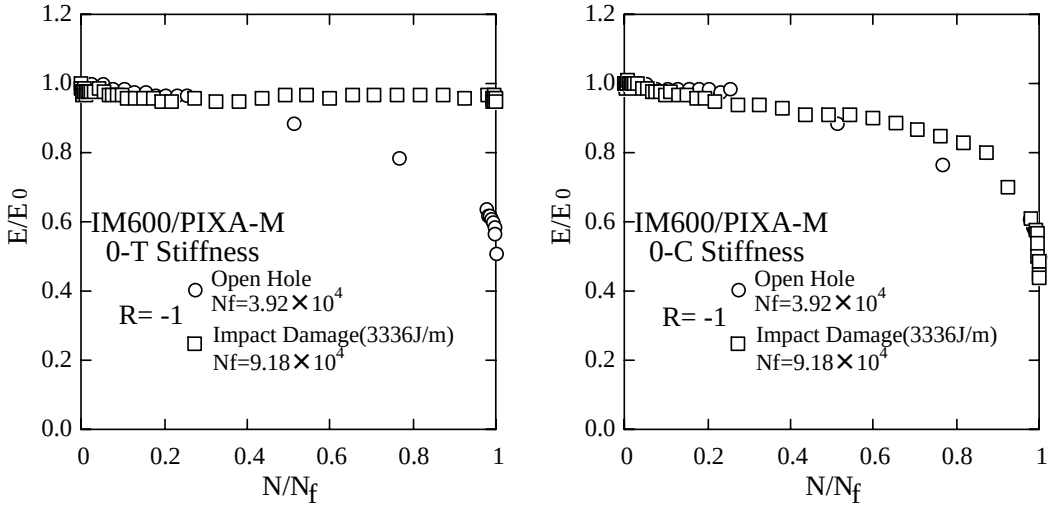

(b)

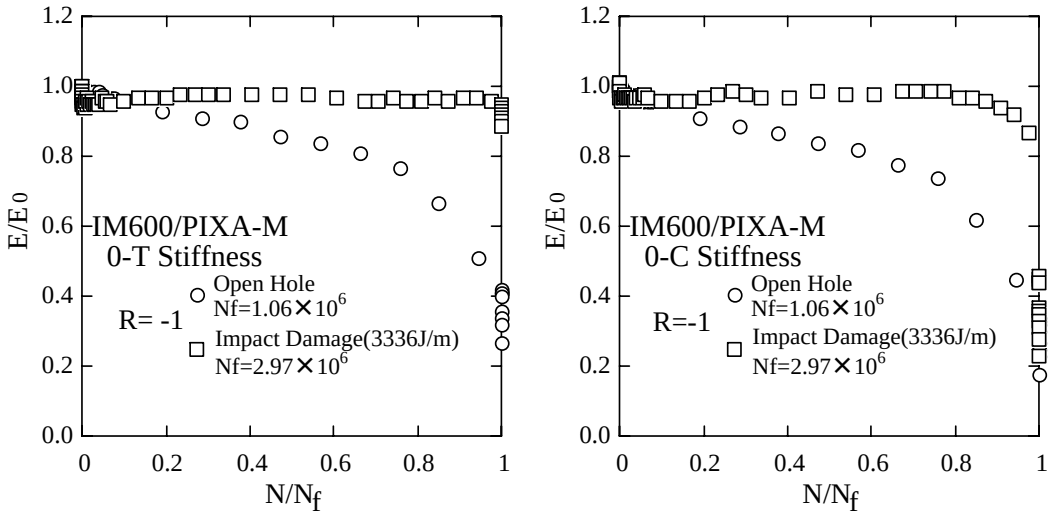

(c)

Fig. 8. Comparisons of normalized stiffness changes for IM600/PIXA-M